

Date of publication xxxx 00, 0000, date of current version xxxx 00, 0000.

Digital Object Identifier 10.1109/ACCESS.2017.DOI

# Improvement of Spiking Neural Network With Bit Planes And Color Models

NHAN T. LUU<sup>1</sup> (MEMBER, IEEE), DUONG T. LUU<sup>2</sup>, PHAM NGOC NAM<sup>3</sup> (MEMBER, IEEE), AND TRUONG CONG THANG<sup>4</sup> (SENIOR MEMBER, IEEE)

<sup>1</sup>College of Information and Communication Technology, Can Tho University, Can Tho, Vietnam

<sup>2</sup>Information and Network Management Center, Can Tho University, Can Tho, Vietnam

<sup>3</sup>College of Engineering and Computer Science, VinUniversity, Hanoi, Vietnam

<sup>4</sup>Department of Computer Science and Engineering, The University of Aizu, Aizuwakamatsu, Japan

Email: luutn@ctu.edu.vn, luutd@ctu.edu.vn, nam.pn@vinuni.edu.vn, thang@u-aizu.ac.jp

arXiv:2410.08229v4 [cs.CV] 18 Oct 2025

**ABSTRACT** Spiking neural network (SNN) has emerged as a promising paradigm in computational neuroscience and artificial intelligence, offering advantages such as low energy consumption and small memory footprint. However, their practical adoption is constrained by several challenges, prominently among them being performance optimization. In this study, we present a novel approach to enhance the SNN for image classification through a new coding method that exploits bit plane representation. Also, we investigate the impacts of color models of the proposed coding process. Through extensive experimental validation, we demonstrate the effectiveness of our coding strategy in achieving performance gain across multiple datasets of grayscale images and color images. To the best of our knowledge, this is the first research that considers bit planes and color models in the context of SNN. By leveraging the unique characteristics of bit planes, we hope to unlock new potentials in SNNs performance, potentially paving the way for more effective SNNs models in future researches and applications.

**INDEX TERMS** Spiking neural network, spike coding, image classification, bit planes, color models

## I. INTRODUCTION

THE field of artificial intelligence (AI) has experienced unprecedented advancements in recent decades [1], largely driven by the developments of deep learning algorithms. Despite these advancements, traditional artificial neural networks (ANNs) often fall short in modeling the intricate and dynamic nature of biological neural systems [2]. To bridge this gap, spiking neural networks (SNNs) have emerged as a promising alternative, leveraging the temporal dimension of neuronal activity to more closely emulate the behavior of biological brains.

SNNs utilize discrete spike events to transmit information between neurons, mirroring the asynchronous and event-driven communication observed in biological neurons [3]. This approach not only enhances the biological plausibility of neural models but also offers potential advantages in terms of computational efficiency and power consumption, particularly for hardware implementations [4]. The inherent sparsity and temporality in coding of SNNs provide a robust framework for developing low-power neuromorphic systems that can operate efficiently in real-time environments [5].

Despite their potential, SNNs pose significant challenges,

particularly in training methodologies and network optimization. Traditional backpropagation techniques used in ANNs are not directly applicable to SNNs due to their discontinuous and non-differentiable nature [6]. Consequently, novel training algorithms, such as spike-timing-dependent plasticity (STDP) [7], [8] and surrogate gradient methods [9]–[11], have been developed to address these challenges, enabling the effective training of SNNs.

Prior research in ANN has explored the application of bit planes (e.g. [12]) and color models [13], [14] to enhance performance across various tasks, demonstrating significant improvements in areas such as image recognition and processing. Motivated by these advancements, we aim to investigate whether bit planes and color models can similarly improve the performance of SNNs. This led us to formulate our research questions:

- *How can we utilize bit plane representation to enhance the performance of SNN?*
- *How can we utilize different color models to enhance the performance of SNN?*

In our research, we observe that bit planes of an image contain pulse-like information, and can be applied to encode

pixel values for SNNs to improve accuracy during surrogate gradient training. Through extensive experiments, it is shown that bit planes contain valuable information that can be utilized in the spike coding process as a supplementary data source for SNN. Also, bit plane coding proves to be reutilized across multiple color models. Furthermore, RGB color model, which is the default color model of many datasets, is not always the best one among the evaluated color models in our study.

A preliminary version of this paper is published in [15], where the benefit of using bit plane coding is proved by three grayscale datasets. In this extended version, the following new points have been added.

- First, the proposed method was updated to support color images.
- Second, eight more datasets were included in the experiments.
- Third, impacts of color models were investigated.
- Fourth, discussion and analysis of the paper were significantly extended.

Table 1: Table of abbreviation (in alphabetical order) used in this paper.

Abbreviation	Full Name
ADD	Addition
ANN	Artificial neural network
CIE	International Commission on Illumination
IF	Integrate-and-fire
LIF	Leaky integrate-and-fire
ReLU	Rectified linear unit
SEW	Spike-element-wise
SNN	Spiking neural network
SNR	Signal-to-noise ratio
STDP	Spike-timing-dependent plasticity

Table 2: Table of algorithmic symbols used in this paper.

Symbol	Meaning
$X$	Input image tensors
$X_{max}$	Integer value indicate the maximum value of input image tensor
$n_{bit}$	Minimum number of bit planes required to encode input $X$ into bit planes
$log_2()$	Binary logarithm function
$X_{shape}$	Dimensions of $X$ , include: <ul style="list-style-type: none"> <li>• <math>B</math>: number of images being processed.</li> <li>• <math>C</math>: number of image channels.</li> <li>• <math>H</math>: image height.</li> <li>• <math>W</math>: image width.</li> </ul>
$concat()$	Tensor concatenation function, concatenating a list of tensors resulted to a tensor contain spikes of shape $(n_{bit}, X_{shape})$
$convertColor()$	Tensor color model converting function, convert $X$ to a specified color model decided by value of $colormodel$
$colormodel$	A string value specify the color model to convert the tensor to (i.e. "RGB", "CMY")
$mod$	Modulo division
$L$	A list-like [16] data structure, used to temporarily store coding result
$\mathbb{Z}$	The set of all integers

## II. SPIKING NEURAL NETWORK

In this section we present an overview of SNN. The abbreviations and algorithmic symbols used throughout the paper are listed in Table 1 and Table 2.

### A. OVERVIEW OF SNNs

SNNs can be considered a biologically inspired variant of ANNs that offer a different computational paradigm. Unlike traditional ANNs, which process information in a continuous manner using floating-point activations and backpropagation-based learning [17], SNNs rely on discrete events called spikes to encode and transmit information [18]. This event-driven nature of SNNs allows for energy-efficient computations, making them suitable for neuromorphic hardware implementations [19]. While the majority of mainstream ANNs architecture operate on floating point data representations, SNNs mimic the sparse, time-dependent processing found in biological neurons [20]. Furthermore, SNNs employ temporal dynamics to learn and process temporal information naturally, leveraging mechanisms such as STDP for unsupervised learning [21]. Despite their advantages, the training of SNNs remains challenging due to the non-differentiable nature of spike events, often necessitating specialized training methods like surrogate gradients [9], [11], [22], hybrid SNN training [23] or ANN-to-SNN conversion approaches [24]. Thus, SNNs present a compelling alternative to ANNs for energy-efficient and biologically plausible computations, while also introducing unique challenges in model design and training.

One of the earliest neuron models that is still widely applied in modern SNN architectures is the perfect integrate-and-fire (IF) model (also sometimes referred to as the non-leaky integrate-and-fire model), first studied by Louis Lapicque in 1907 [25]. In this model, the neuron is characterized by its membrane potential  $V$ :

$$C \frac{dV(t)}{dt} = I(t) \quad (1)$$

which evolves over time in response to an input current  $I(t)$ . This evolution is described by the time derivative of the capacitance law,  $Q = CV$ , where  $C$  is the membrane capacitance. As an input current is applied, the membrane potential increases until it reaches a fixed threshold  $V_{th}$ . At this point, the neuron generates a spike modeled as a delta function, and the membrane potential is reset to its resting value, after which the process repeats. In this model, the firing rate increases linearly and indefinitely with the increase in input current.

While previous efforts have successfully converted ANN neurons with ReLU activations to IF neurons [26]–[28], challenges still remain in the conversion process. One of the key issues is the difficulty in precisely determining the appropriate thresholds in these conversion approaches. Despite the introduction of both data-driven and model-driven threshold determination methods [29], the converted SNN often experience unstable accuracy compared to their re-trained ANN

counterparts. Additionally, IF neurons lack time-dependent memory. Once a neuron receives sub-threshold potentials, the membrane potential persists without decay until the neuron fires. This behavior is said to be inconsistent with biological neurons, which exhibit dynamic temporal properties [30].

Still, recent study have shown that SNN employed with IF neurons are more energy efficient than traditional ANN [31]. Within certain SNN architectures, IF neurons have demonstrated superior performance compared to the supposedly better than leaky integrate-and-fire (LIF) neurons [30], with the SEW-ResNet [11] architecture being one such example.

### B. DEEP RESIDUAL LEARNING IN SNNS

The success of ResNet [33] in deep learning has motivated efforts to extend residual learning to SNN. Prior attempts, commonly referred to as Spiking ResNets [28], have largely replicated the architecture of ResNet [33] by replacing ReLU activation functions with spiking neurons. However, this approach presents certain limitations:

- *Inability to achieve identity mapping across neuron models*: Residual learning is predicated on the concept of identity mapping, where layers can be trained to approximate an identity function. While this is straightforward in ResNets [33] with ReLU activation, it is not always feasible in Spiking ResNets [28]. Specifically, [11] claimed that for certain spiking neuron models, such as LIF neurons [25] with learnable membrane time constants, ensuring that a spiking neuron fires in response to an input spike becomes challenging. This complicates the realization of identity mapping.
- *Vanishing/exploding gradients*: Even in cases where identity mapping can be achieved, Spiking ResNets [28] are prone to vanishing or exploding gradients during training. This occurs because the gradient propagation through multiple layers of spiking neurons may either diminish to zero or grow uncontrollably, complicating the training of deeper networks.

To address these issues, SEW ResNet [11] was introduced as a replacement design for residual blocks while utilizing IF neurons. The SEW block capitalizes on the binary nature of spikes by applying element-wise functions  $g$  to the output of the residual mapping  $A_l[t]$  and the input spike train  $S_l[t]$  [11]. This approach facilitates identity mapping, mitigates the vanishing/exploding gradient problem and achieves higher accuracy with fewer time steps compared to existing SNN models.

In recent researches, using backpropagation methods to train SNNs [9]–[11], [34] has become a common practice in neuromorphic computing. In SNNs, spike signals are typically modeled using binary values (0s and 1s) from a Heaviside function  $H(\theta, t)$ , where  $\theta$  is the membrane potential and  $t$  is a threshold:

$$H(\theta, t) = \begin{cases} 1 & \text{if } \theta - t \geq 0 \\ 0 & \text{otherwise} \end{cases} \quad (2)$$

The derivative  $\partial H$  of this function is given by:

$$\frac{\partial H}{\partial \theta} = \begin{cases} +\infty & \text{if } \theta - t = 0 \\ 0 & \text{otherwise} \end{cases} \quad (3)$$

As shown, directly differentiating  $H(\theta, t)$  results in unstable gradients. To address this, we can substitute the derivative of the Heaviside function  $\partial H$  with a numerically stable gradient from a different activation function during backpropagation, such as the derivative  $\partial \sigma$  of the Sigmoid function  $\sigma(\theta, t)$ :

$$\sigma(\theta, t) = \frac{1}{1 + e^{\theta-t}} \quad (4)$$

$$\frac{\partial H}{\partial \theta} = \frac{\partial \sigma}{\partial \theta} = \frac{e^{\theta-t}}{(e^{\theta-t} + 1)^2}$$

This approach yields a more stable gradient during backpropagation, allowing the use of existing automatic differentiation frameworks to optimize SNNs effectively [11].

Similar to other new types of neural networks [35]–[37], the choice of input data representation may have strong impacts on output performance. Thus, in this paper we investigate a new way that employs bit plane coding for data representation in SNNs.

## III. BIT PLANES AND COLOR MODELS IN DEEP LEARNING

This section presents an overview of bit planes and color models, along with their applications in deep learning algorithms.

### A. BIT PLANES IN DEEP LEARNING

In the context of digital discrete signals such as images, a bit plane represents the collection of bits that occupy the same position within the binary representation of the signal's numerical values (as illustrated in Figure 1). For instance, in a 8-bit data representation, there are 8 distinct bit planes. The 1<sup>st</sup> bit plane consists of the most significant bits, while the 8<sup>th</sup> bit plane comprises the least significant bits. The first bit plane provides the coarsest yet most fundamental approximation of the signal's values. As the bit plane index increases, its contribution to the overall representation diminishes. Consequently, incorporating additional bit planes progressively refines the signal's approximation.

Bit planes have shown extensive utility in deep learning applications, offering new ways to improve model efficiency and performance. In [12], researchers used bit planes to encode the input layer in Binary Neural Network (BNN). They argued that bit planes retain crucial spatial information, enabling a reduction in the number of multiply-accumulate operations (MACs) without compromising the model's accuracy or robustness. This demonstrates the potential of bit planes in streamlining computations while maintaining competitive performance.

The use of bit plane slicing on RGB images for adversarial robustness was explored in [38]. By selecting the most

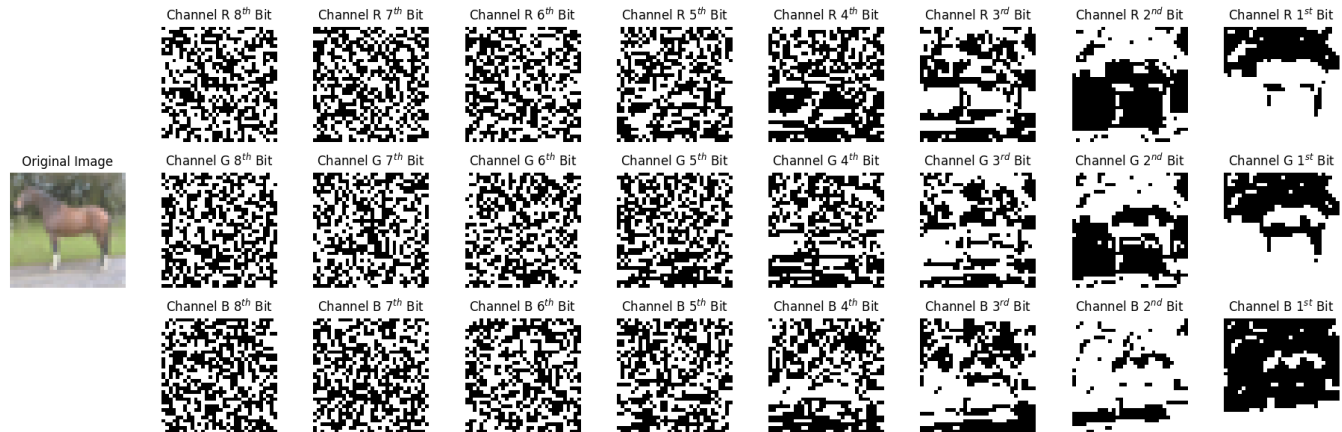


Figure 1: Visualization of the extracted bit planes from a sample image in the CIFAR-10 dataset [32]. Higher-order bit planes (e.g., most significant bits) encode more spatial and structural information, capturing the prominent features of the image. In contrast, lower-order bit planes (e.g., least significant bits) primarily contain finer details and noise, contributing less to the overall image structure.

significant bit planes, the authors developed a classification model that was better equipped to handle adversarial attacks. This approach capitalizes on the spatial information encoded in different bit planes, which helps the model resist manipulations that would otherwise degrade its performance.

In the domain of medical imaging, bit plane slicing has also been applied to improve accuracy in breast cancer recognition tasks [39]. Researchers found that lower-order bit planes are more susceptible to noise, and by removing them before inputting the data into a convolutional neural network (CNN), they achieved higher classification accuracy. This method highlights how bit plane analysis can be tailored to specific challenges, such as noise reduction in medical images, to enhance model effectiveness.

Although bit planes have been widely studied and applied in ANNs, their utilization in SNNs is still unexplored. As far as we are concerned, our research is first to explore application of bit planes on SNNs spike coding process.

### B. COLOR MODELS IN DEEP LEARNING

Color models are fundamental in computer graphics as they define how colors are represented, manipulated, and displayed for digital images. In computer graphics applications, understanding and effectively managing color models is crucial for tasks such as rendering realistic scenes, creating digital artwork, and designing user interfaces. Color models can be divided into *device-oriented models*, *user-oriented models* and *device-independent models* [40], [41].

Device-oriented color models are influenced by the signals of the devices and the resulting colors are affected by the technology used for display. Widely utilized in various applications that require color consistency with hardware tools, examples include any hardware devices used for human visual perception, such as televisions and video systems. Popular color models for devices include RGB, CMY(K) and YCbCr.

User-oriented color models are considered as a pathway between the observer and the device handling the color information. For our study, we mostly investigate cylindrically described models, including HSL and HSV. According to [40], these models also inherit other special properties such as device dependence and cylindrical-coordinate representation.

Device-independent color models are essential for defining color signals without reliance on the specific characteristics of any particular device or application. These models play a crucial role in applications that involve color comparisons and the transmission of visual information across networks that connect various hardware platforms. We will mostly research color models defined by the International Commission on Illumination (CIE), including CIE XYZ and CIE LAB.

Color models are becoming increasingly important in deep learning algorithms, offering valuable information that enhances model performance in various tasks, such as image recognition [13], [42], image segmentation [14] and adversarial attacks prevention [43].

Despite extensive researches on the use of color models in ANN, their application in SNN remains unexplored and requires further investigation.

### IV. PROPOSED METHOD

In this section, we present in detail the design of our coding algorithm.

We hypothesize that the information contained in the bit planes of an image can be effectively used to encode inputs for SNN training. Bit planes decompose an image into binary levels, each representing a specific bit of the binary representation of pixel values. This decomposition can potentially preserve critical information of the original image while providing a format that might be more suitable for the spike-based processing in SNNs. The granularity of information available in bit planes offers a unique approach to encoding

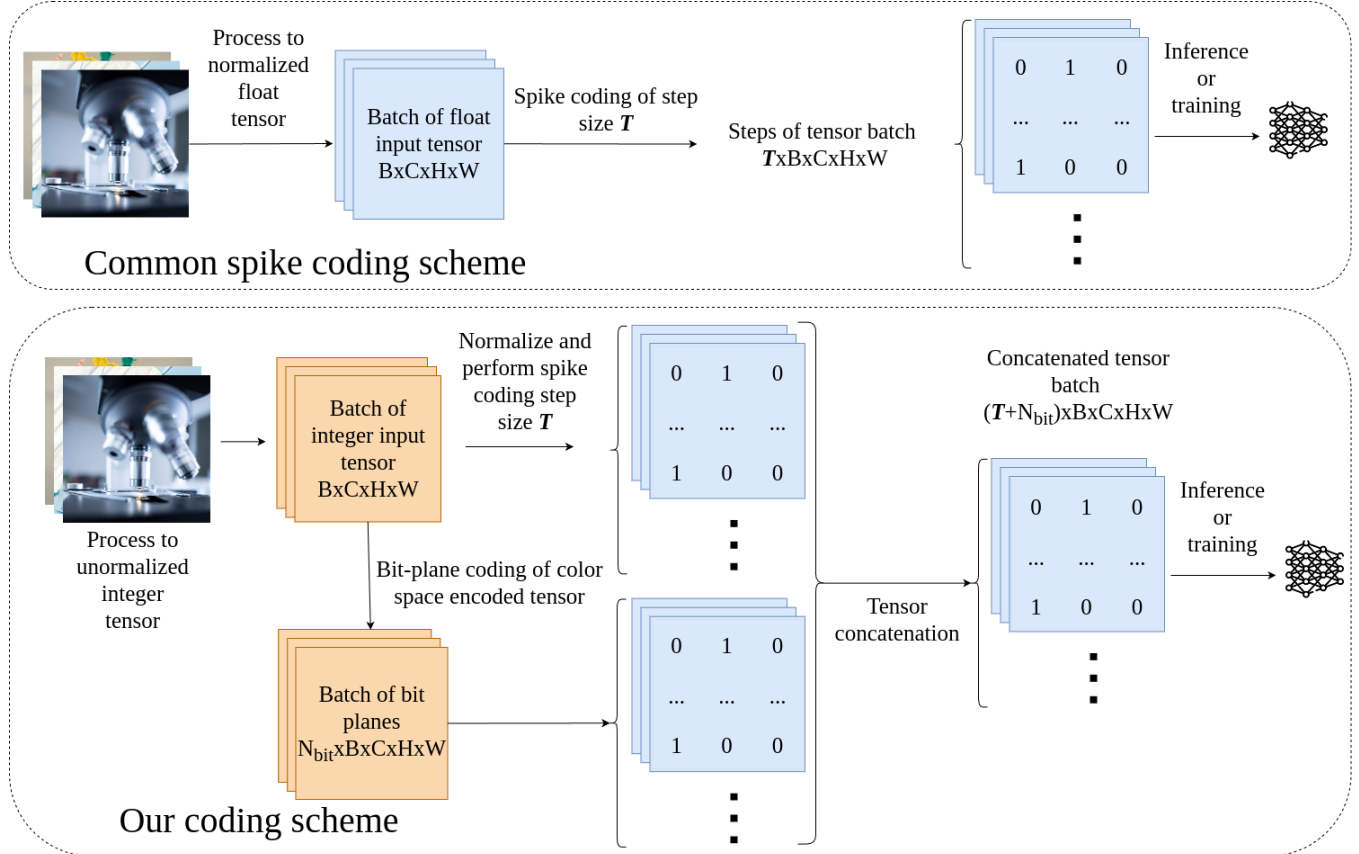


Figure 2: Our proposed coding method (lower) compare with traditional spike coding method (upper).

visual data, which could enhance the learning capabilities of SNNs by providing a richer, multi-level representation of the input.

To test this hypothesis, we conducted a preliminary experiment and analysis using the MNIST [44], which is a simple dataset containing grayscale images of hand-written numbers. We compared three approaches: traditional rate coding, bit plane coding only, and the combination of both rate coding and bit plane coding. The detailed settings of this experiment can be found in Section VI-A. The results are provided in Table 3.

Table 3: Average validation accuracy comparison on MNIST [44]

Coding method	Validation Accuracy (%)
Rate coding	98.62
Bit plane coding only	97.87
Combination of rate coding and bit plane coding	<b>98.93</b>

We can see that the accuracy when using exclusively bit-plane-encoded inputs is lower compared to the baseline. However, a combination of rate coding and bit-plane coding resulted in an increase in performance. This outcome demonstrates that bit planes contain valuable information that SNN can learn from to improve their classification ability. This

encourages us to carry out a further study and perform testing on other datasets.

As we can see in Figure 2, the proposed coding scheme integrates a dual approach featuring both traditional spike coding and bit plane coding. Initially, the process commences with the conventional spike coding procedure applied to the image tensor. The bit plane coding algorithm is then employed to transform an input image into binary planes. The final encoded tensors are then generated through tensor concatenation across the first dimension, merging the outputs from spike coding and bit plane coding. These encoded tensors are thereby prepared for utilization in inference tasks and/or training processes.

The process of converting a multi-channel image into its bit planes involves isolating each bit of the binary representation of the pixel values for each color channel. For an  $n_{bit}$  image, let  $I_C(x, y)$  denote the intensity of a pixel at position  $(x, y)$  for a given color channel  $C$ , pixel intensity can be expressed in terms of its binary representation as:

$$I_C(x, y) = \sum_{k=0}^{n_{bit}} B_{k,C}(x, y) \cdot 2^k \quad (5)$$

where  $B_{k,C}(x, y) \in \{0, 1\}$  is the  $k$ -th bit of the binary representation of  $I(x, y)$ , and  $k$  represents the bit-plane index,

with  $k = 0$  corresponding to the least significant bit and  $k = n_{bit}$  corresponding to the most significant bit.

To isolate a specific bit-plane, the  $k$ -th bit of the pixel can be extracted using the following equation:

$$B_{k,C}(x, y) = \left\lfloor \frac{I_C(x, y)}{2^k} \right\rfloor \bmod 2 \quad (6)$$

---

**Algorithm 1** Bit plane coding algorithm

---

```

Require:  $X_{max}$  is defined,  $X_{max} > 0$  and  $X \in \mathbb{Z}$ 
function BITPLANEENCODE( $X, X_{max}, \text{colormodel}$ )
     $X = \text{convertColor}(X, \text{colormodel})$   $\triangleright$  Convert  $X$  to
    specified color model
     $n_{bit} \leftarrow \lceil \log_2(X_{max}) \rceil$   $\triangleright$  Get number of bit required to
    encode image from highest possible value  $X$ 
     $L \leftarrow []$   $\triangleright$  Empty list initialization
    for each  $X_{shape}.C$  do
        for  $i \leftarrow 0, i < n_{bit}, i + +$  do
             $L.insert(X \bmod 2)$   $\triangleright$  Element-wise modulo
            of tensor, then store the bit plane to  $L$ 
             $X \leftarrow \lfloor X/2 \rfloor$   $\triangleright$  Element-wise division of input
            image tensor and floor the result
        end for
    end for
    return  $\text{concat}(L)$   $\triangleright$  Concatenate all stored sub
    tensors in  $L$  to a single tensor
end function

```

---

To encode an image tensor batch  $X$  into  $n_{bit}$  bit planes in our training process based on established knowledge, we implement Algorithm 1. It is essential to know the maximum possible value  $X_{max}$  of the tensor batch in order to determine  $n_{bit}$ . Since different color models have different  $X_{max}$ , this value must be predefined according to the selected color model. Once  $X_{max}$  is defined,  $n_{bit}$  can be calculate as:

$$n_{bit} = \lceil \log_2(X_{max}) \rceil \quad (7)$$

Bit planes calculation of an unnormalized integer input tensor batch  $X$  can be performed by element-wise division of  $X$  by 2. The remainder from this division constitutes a bit plane of  $X$ , while the quotient is saved for the extraction of subsequent bit planes. This process is repeated until we obtain  $n_{bit}$  bit planes. The resulting bit planes are then concatenated to form  $n_{bit}$  binary tensor batch of  $X_{shape}$ . This format closely resembles that of rate coding and ensures determinism in the coding results without having to sample more than  $n_{bit}$  times.

## V. THEORETICAL BASIS

In this part, we aim to establish a theoretical foundation for our proposed method of spike coding within surrogate gradient approaches.

As discussed in Section II-B, surrogate gradient methods attempt to adapt deep learning's gradient optimization techniques to SNNs, maintaining a close connection to traditional deep learning and convex optimization. A classical stochastic

optimization problem associated with learning a target function  $h$  can be formulated as [45]:

$$\min_{\mathbf{w}} F_h(\mathbf{w}) = \mathbb{E}_{\mathbf{x}} [\ell(p_{\mathbf{w}}(\mathbf{x}), h(\mathbf{x}))], \quad (8)$$

where  $\ell$  is a loss function,  $\mathbf{x}$  represents stochastic inputs (assumed to be vectors in Euclidean space), and  $p_{\mathbf{w}}$  is a differentiable predictor parameterized by  $\mathbf{w}$ . It is assumed that  $\mathbb{E}_{\mathbf{x}} [\|\frac{\partial}{\partial \mathbf{w}} p_{\mathbf{w}}\|^2] \leq G(\mathbf{w})^2$  for some scalar  $G(\mathbf{w})$ , and that  $F$  is differentiable [45], [46].

By reformulating our surrogate gradient optimization process as a traditional stochastic optimization problem, our objective can be defined as:

$$\begin{aligned} \min_{\mathbf{w}} F_h(\mathbf{w}) &= \mathbb{E}_{\mathbf{x}} [\ell(P_{\mathbf{w}}(\mathbf{x}), h(\mathbf{x}))], \\ P_{\mathbf{w}}(\mathbf{x}) &= \mathbb{E}_T [p_{\mathbf{w}}(e(\mathbf{x}))], \end{aligned} \quad (9)$$

where the surrogate gradient model  $P_{\mathbf{w}}(\mathbf{x})$  encodes the input  $\mathbf{x}$  into a spike signal using an encoding function  $e(\mathbf{x})$  and computes the expected output signal across the time dimension  $T$  to generate the final stochastic prediction (basis for this statement can be found ar Appendix A).

Previous studies in gradient-based optimization [45], [46] have demonstrated a positive correlation between a model's performance and the signal-to-noise ratio (SNR) of the stochastic gradient, defined by:

$$\begin{aligned} \text{SNR}(\delta(\mathbf{x})) &= \frac{\text{Sig}(\delta(\mathbf{x}))}{\text{Noi}(\delta(\mathbf{x}))}, \\ \text{Sig}(\delta(\mathbf{x})) &= \|\mathbb{E}_{\mathbf{x}} [\delta(\mathbf{x})]\|^2 \\ \text{Noi}(\delta(\mathbf{x})) &= \mathbb{E}_{\mathbf{x}} \|\delta(\mathbf{x}) - \mathbb{E}_{\mathbf{x}} [\delta(\mathbf{x})]\|^2 \\ \delta(\mathbf{x}) &= h(\mathbf{x}) \cdot g_{\mathbf{w}}(\mathbf{x}) \end{aligned} \quad (10)$$

where  $g_{\mathbf{w}}(\mathbf{x}) = \frac{\partial}{\partial \mathbf{w}} p_{\mathbf{w}}(\mathbf{x})$  is the Jacobian of model  $p_{\mathbf{w}}(\mathbf{x})$  with respect to model weight  $\mathbf{w}$ . Since this correlation does not depend on input gradient calculation, we can directly apply this in our research.

Upon performing signal concatenation using bit-plane-based signal  $B$  of bit length  $N_{bit}$  as in the proposed method, given certain condition satisfied, we can have:

$$\begin{aligned} \sup(SNR(\delta^{bit}(\mathbf{x}))) &\geq \sup(SNR(\delta(\mathbf{x}))), \\ \sup(SNR(\delta^{bit}(\mathbf{x}))) &= \frac{\|\mathbb{E}_{\mathbf{x}} [\delta^{bit}(\mathbf{x})]\|_{\infty}^2}{\mathbb{E}_{\mathbf{x}} \|\delta^{bit}(\mathbf{x}) - \mathbb{E}_{\mathbf{x}} [\delta^{bit}(\mathbf{x})]\|_{\infty}^2}, \\ \sup(SNR(\delta(\mathbf{x}))) &= \frac{\|\mathbb{E}_{\mathbf{x}} [\delta(\mathbf{x})]\|_{\infty}^2}{\mathbb{E}_{\mathbf{x}} \|\delta(\mathbf{x}) - \mathbb{E}_{\mathbf{x}} [\delta(\mathbf{x})]\|_{\infty}^2} \end{aligned} \quad (11)$$

and improving the chance of obtaining higher SNR (more background details and proof for Equation 11 can be found at Appendix B).

To empirically validate our hypothesis, we measure the gradient SNR of the model across all training epochs on MNIST dataset (since to ensure that gradient does not saturate during training,  $p_{\mathbf{w}}(\mathbf{x})$  should serves as a reasonable approximation of the target function  $h(\mathbf{x})$ ). The resulted SNR measurements across all training epochs are presented in

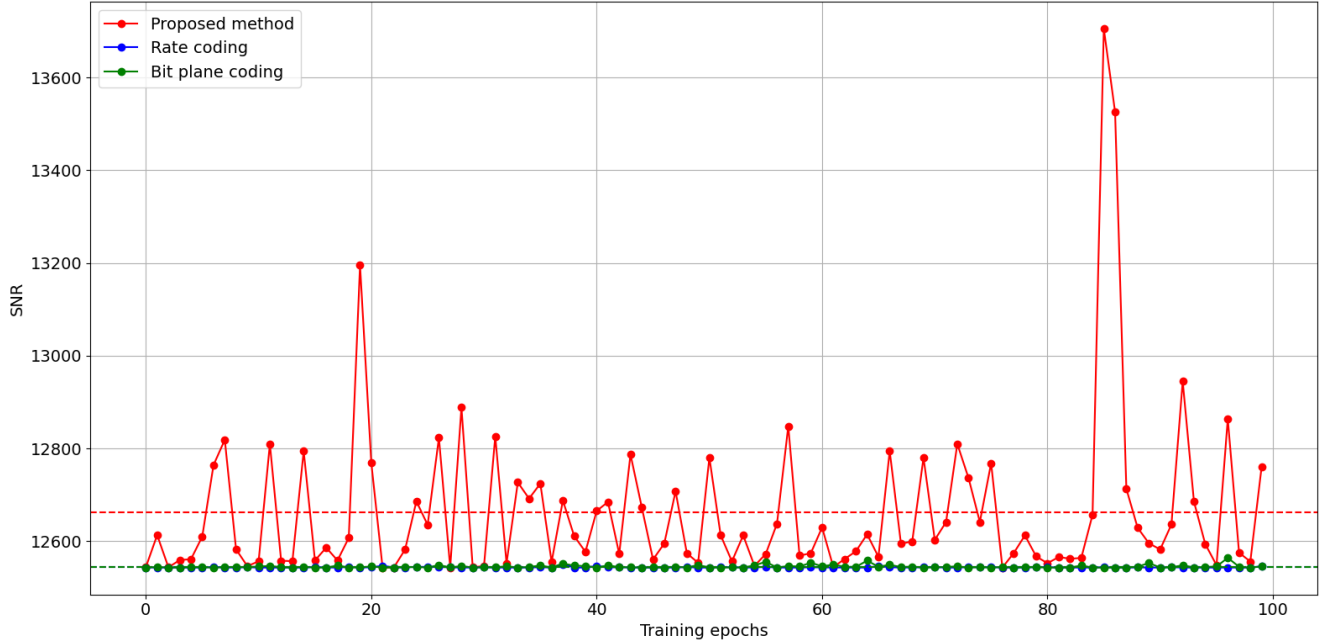


Figure 3: Comparing model gradient's SNR of the proposed method (red), baseline (blue) and bit plane coding (green) of MNIST dataset across the epochs. Dashed line indicate the mean gradient SNR (higher is better based on our assumption).

Figure 3. The findings demonstrate that our proposed method achieves a higher mean SNR during training process, which aligns with our initial assumption.

## VI. EXPERIMENTS

### A. EXPERIMENTAL SETTINGS

To investigate performance of SNN for images, we employed the popular tool SEW-ResNet18 with ADD element-wise function [11]. The model and experiment process were implemented using PyTorch [47] and SpikingJelly [48]. Color conversion algorithms are based on implementations from Kornia [49]. For the baseline method in the experiments, the *Poisson-distributed rate coding* [50], [51] is employed with a step size  $T = 10$  where spike  $s_{T,i}$  for  $i$ -th pixel at step  $T$  with intensity  $P_{T,i}$  can be interpreted as:

$$s_{T,i} = \begin{cases} 1 & \text{if } \text{random}(0.0, 1.0) \leq P_{T,i} \\ 0 & \text{otherwise} \end{cases} \quad (12)$$

To enable efficient training, surrogate gradient methods were applied to all IF neurons. We utilized the arctangent surrogate gradient function  $S(U)$  [10], [11]. Also, we adopted the standard cross-entropy loss function with a softmax activation, commonly adopted for classification tasks [47], [52], [53], computed using mean reduction across mini-batches.

Inspired by traditional deep learning approach in model fine-tuning [52], [53], the optimization process is conducted with the Adam algorithm [54], using a learning rate of  $lr = 1 \times 10^{-3}$  and parameters  $\beta = (0.9, 0.999)$  across all evaluated datasets.

In the first part of our experiments, we only use grayscale image datasets to clearly see the effects of bit plane coding. In the second part, popular datasets of color images are used to see the practical effects of both bit plane coding and color models. We allocated 80% of each dataset for training and the remaining 20% with deterministic random seeding for validation. All datasets were processed with a batch size of 16 images for 100 epochs on an NVIDIA RTX 3090 GPU.

### B. EXPERIMENTAL RESULTS

In this part, we will discuss results of our main experiments along with some interesting findings beside original hypotheses.

1) The effect of bit plane coding on grayscale image datasets

Table 4: Comparison of validation accuracy among coding methods. Best performances on each dataset are denoted in bold. Performance gain when compared with the baseline is highlighted in green.

Dataset	Accuracy of coding methods (%)		
	Baseline	Bit plane coding	Proposed method
MNIST [44]	98.62	97.87	<b>98.93 (+0.31)</b>
KMNIST [55]	94.13	92.33	<b>95.58 (+1.45)</b>
Fashion-MNIST [56]	88.83	86.66	<b>90.19 (+1.36)</b>
<b>Average</b>	93.86	92.29	<b>94.90 (+1.04)</b>

First, we aim to investigate whether the proposed approach yields any significant or insightful results without impacts of color information. For that, we employed three popular

datasets of grayscale images, including MNIST [44], KMNIST [55], Fashion-MNIST [56]. The results of MNIST dataset were already shown in Table 3. However, they are still included here to see the behaviors of the coding methods over different datasets. As grayscale images consist of only intensity values ranging between [0, 255], we apply our coding process with one channel. This process would produce 8 bit-plane channels that represent the image information in binary form. In this part, we investigate three options, namely:

- the baseline model (spike coding only),
- using bit plane coding only,
- the proposed model (spike coding combined with bit plane coding).

As demonstrated in Table 4, the combination of spike coding with bit-plane coding outperformed other coding methods in terms of validation accuracy. As mentioned, using only bit-plane coding resulted in a reduction in accuracy; however, the combination of spike coding with bit plane coding (i.e. the proposed method) provides gain in all datasets. For any method, the accuracy value is highest with the MNIST dataset and lowest with the Fashion-MNIST dataset. This could be because among these three datasets, MNIST is the simplest one while Fashion-MNIST is the most complex one. Interestingly, the gain of the proposed method compared to the baseline is increased from 0.31% (with MNIST) to roughly 1.45% (with KMNIST) and averaged at 1.04%. That means the impact of bit plane coding is more prominent with more complex datasets.

## 2) Comparison of SNN variants

In addition, we also evaluated our spike coding scheme in different SNN variants. We employ only both grayscale and color image datasets in this part, including MNIST, KMNIST, Fashion-MNIST and CIFAR10. We benchmarked against multiple variants of Spiking ResNet [28] with LIF surrogate neurons, which have demonstrated competitive performance in prior work, along with AND and IAND variants of SEW-ResNet18 [11].

In shown in Table 5, the results reveal that in all of the tested variants, the proposed method consistently achieves a higher accuracy than the baseline. The performance gains range from 0.31% (in the case of SEW-ResNet18 (ADD) on MNIST dataset) to 44.40% (in the case of Spiking-ResNet50 on Fashion-MNIST). Also, Spiking-ResNet variants tend to underperform when compared with SEW-ResNet18 variants. The average accuracy values across all datasets show that SEW-ResNet18 (ADD) is the best variant. Fang *et al.* [11] also demonstrated that this variant usually achieves superior performance. Therefore, in subsequent experiments, we exclusively utilize this variant for benchmarking.

## 3) The effect of bit plane coding on color images

For our experiment, we conducted tests on various color-image classification datasets, including CIFAR10 [32], CIFAR100 [32], EuroSAT [59], Caltech101 [57], Caltech256

[58], Imagenette [60] (which is a subset of ImageNet [62]) and Food101 [61]. The default color model of these datasets is RGB. Due to computing resource constraints of the simulation tool, large images are downsampled to 224x224 pixels. So, among these datasets, CIFAR10 [32], CIFAR100 [32] and EuroSAT [59] are trained with original input size while images of all other dataset are resized to 224x224 pixels.

The accuracy results of different cases are shown in Table 6. We can see that, the accuracy of the proposed method is always higher than that of the baseline. The gain ranges from the lowest of 2.80% (with CIFAR100) up to 17.33% (with Food101 dataset), depending on the employed dataset. This suggests that the benefit of the proposed method when applying to color images is more significant than when applying to grayscale images.

## 4) Impacts of color models

In this part, we investigate the effect of color models on the performance of proposed method. The results are provided in Table 7 and also visualized in Fig. 4. In this figure, the baseline model is also included for the sake of comparison. From Fig. 4, it can be seen that our proposed method using different color models is consistently better than the baseline. Also, in general, the variations in performances of different color models are small.

From Table 7, the results show that RGB is not always the best color model. Among the eight datasets, RGB provides the best performance in only 2 cases (namely CIFAR100 and Caltech256). CMY does not achieve any best results, whereas each of the other five color models achieves the best performance once. Especially, with Caltech101 dataset, the accuracy of HSV color model is 68.41%, which is considerably higher than that of RGB color model (64.55%).

When averaging the accuracy values across all datasets, the HSL color model slightly outperforms the others for both coding method, as indicated in the last row of Table 7. The CMY color model, which does not achieve any best results, also has the lowest average performance. Further analysis reveals a distinctive characteristic of the HSL model that may contribute to its relatively stable performance. HSL encodes the hue component using a 0–359 degree representation, which results in a higher number of spike counts. Consequently, the maximum number of bits required for representation increases to  $n_{bit} = 9$ . As theoretically formulated in Section V, this greater bit depth might facilitates a higher SNR ratio that enables better performance. In contrast, the CMY model operates within a more limited range of [0, 100] and thus needs only  $n_{bit} = 7$  bits to represent the color values. Based on the same logic of Section V, this smaller number of bits reduces the gradient magnitude along with signal term for model SNR and thus results in its lower performance.

To rigorously quantify the computational overhead introduced by our method with different color models, we measure the running times of an image batch on forward propagation for both baseline and the proposed method. As

Table 5: Comparison of validation accuracy of the baseline and the proposed method on different SNN variants. Performance gain when compared with the baseline is shown in green and best performing model on average is denoted in bold.

SNN variant	Accuracy of coding methods per dataset(%)									
	MNIST		Fashion-MNIST		KMNIST		CIFAR10		Average	
Base-line	Proposed method	Base-line	Proposed method	Base-line	Proposed method	Base-line	Proposed method	Base-line	Proposed method	
SEW-ResNet18 (ADD)	98.62	98.93 ( <b>+0.31</b> )	94.13	95.58 ( <b>+1.45</b> )	88.83	90.19 ( <b>+1.36</b> )	70.69	73.49 ( <b>+2.80</b> )	88.07	<b>89.55</b> ( <b>+1.48</b> )
SEW-ResNet18 (AND)	97.41	98.48 ( <b>+1.07</b> )	87.14	89.14 ( <b>+2.00</b> )	90.13	94.26 ( <b>+4.13</b> )	62.58	70.95 ( <b>+8.37</b> )	84.32	88.21 ( <b>+3.89</b> )
SEW-ResNet18 (IAND)	98.39	98.76 ( <b>+0.38</b> )	88.92	90.15 ( <b>+1.23</b> )	93.23	94.90 ( <b>+1.67</b> )	67.28	71.40 ( <b>+4.12</b> )	86.96	88.80 ( <b>+1.84</b> )
Spiking-ResNet18	98.25	98.74 ( <b>+0.49</b> )	87.47	89.37 ( <b>+1.90</b> )	93.23	95.06 ( <b>+1.83</b> )	46.15	61.79 ( <b>+15.1</b> )	81.28	86.24 ( <b>+4.96</b> )
Spiking-ResNet34	69.02	92.77 ( <b>+23.8</b> )	69.59	79.62 ( <b>+10.0</b> )	37.45	72.23 ( <b>+34.8</b> )	19.28	32.29 ( <b>+13.0</b> )	48.84	69.23 ( <b>+20.4</b> )
Spiking-ResNet50	13.45	46.22 ( <b>+32.8</b> )	12.80	57.20 ( <b>+44.4</b> )	10.44	23.87 ( <b>+13.4</b> )	17.94	27.78 ( <b>+9.84</b> )	13.66	38.77 ( <b>+25.1</b> )

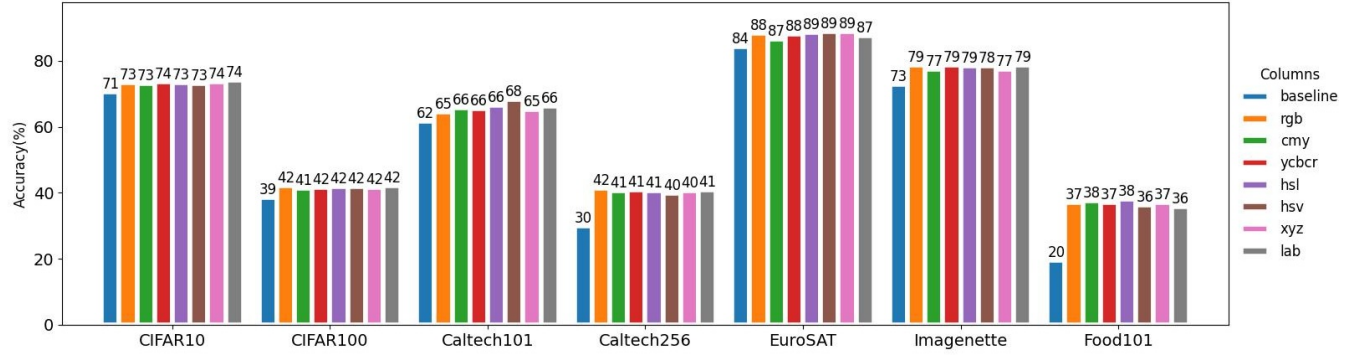


Figure 4: Validation accuracy visualization of proposed method among color models.

Table 6: Average validation accuracy on various computer vision dataset of our proposed method. Best performances are denoted in bold. Performance gain when compare with the baseline is highlighted in green.

Dataset	Accuracy of coding methods (%)		
	Baseline	Bit plane coding	Proposed method
CIFAR10 [32]	70.69	37.28	<b>73.49</b> ( <b>+2.80</b> )
CIFAR100 [32]	38.57	11.28	<b>42.15</b> ( <b>+3.58</b> )
Caltech101 [57]	61.67	43.28	<b>64.55</b> ( <b>+2.88</b> )
Caltech256 [58]	30.04	21.75	<b>41.51</b> ( <b>+11.47</b> )
EuroSAT [59]	84.39	79.87	<b>88.48</b> ( <b>+4.09</b> )
Imagenette [60]	72.99	48.20	<b>78.68</b> ( <b>+5.69</b> )
Food101 [61]	19.62	6.29	<b>36.95</b> ( <b>+17.33</b> )
<b>Average</b>	53.99	35.42	<b>60.83</b> ( <b>+6.84</b> )

shown in Table 8, the increases in running times depend on datasets and color models, ranging from 20.52% (with CIFAR-10 dataset and CMY color model) to 105.01% (with CIFAR-10 dataset and HSL color model). Averaging over all datasets, the increases are from 48.57% (with CMY color model) to 85.35% (with HSL color model).

Figure 5 shows the relationship between the average gain in accuracy and the average increase in processing time for different color models. We can see that any gain in performance requires some increase in processing time. Interestingly, while having the smallest performance gain, the CMY color model also has the lowest processing time increase. In contrast, the HSL color model has the greatest gain as well

as the highest increase in processing time.

### C. DISCUSSION

Based on these observations, the key findings of our analysis are summarized as follows:

- The proposed method yields performance improvements for both grayscale and color images by increasing gradient magnitude and improve model SNR during training process.
- The gain of the proposed method depends on the employed dataset, ranging from 0.31% to 1.45% in small grayscale image dataset and 2.80% to 17.33% for practical colored image dataset with RGB-based variants.
- Proposed method can be generalized for different SNN variants.
- Though RGB is the default color model in existing datasets, it is not always the best one, providing highest results in only two datasets.
- Based on both theoretical foundation and in terms of average accuracy value over all datasets, HSL is the best color model and CMY is the worst one. Yet HSL provides the best performance in only one dataset.

Our experimental results demonstrate that bit-plane coding can enhance the performance of SNNs. Despite the significant performance gains, the added computational complexity is a limitation of our method. As shown in Figure 5, the average complexity increase in terms of processing time can be from 48.57% to 85.35%, which could be a drawback in some applications. Still, along with most spike coding

Table 7: Validation accuracy comparison of proposed method among color models.

Dataset	Accuracy of coding methods (%)						
	With RGB encoded (Ours)	With CMY encoded (Ours)	With YCbCr encoded (Ours)	With HSL encoded (Ours)	With HSV encoded (Ours)	With CIE XYZ encoded (Ours)	With CIE LAB encoded (Ours)
CIFAR10 [32]	73.49	73.73	73.64	73.39	73.06	73.63	<b>74.06</b>
CIFAR100 [32]	<b>42.15</b>	41.31	41.62	41.94	41.91	41.73	42.03
Caltech101 [57]	64.55	65.65	65.53	66.46	<b>68.41</b>	65.30	66.22
Caltech256 [58]	<b>41.51</b>	40.65	40.84	40.55	39.94	40.50	40.79
EuroSAT [59]	88.48	86.61	88.11	88.74	88.81	<b>88.87</b>	87.48
Imagenette [60]	78.68	77.35	<b>78.78</b>	78.55	78.50	77.35	78.70
Food101 [61]	36.95	37.71	36.98	<b>38.03</b>	36.41	37.10	35.87
<b>Average</b>	60.83	60.43	60.79	<b>61.09</b>	61.01	60.64	60.74

Table 8: Comparison of model total forward and backward propagation time between baseline and proposed method using different color models. The values are average training times per epoch per images batch of 16

Model Variants	Processing time by dataset (ms)							
	CIFAR-10	CIFAR-100	Caltech101	Caltech256	EuroSAT	Imagenette	Food101	Average
Baseline	41.67	43.55	141.25	146.92	66.05	135.71	140.66	102.26
Proposed (RGB)	63.66 (+52.77%)	65.39 (+50.15%)	235.13 (+66.46%)	240.41 (+63.63%)	116.77 (+76.79%)	225.83 (+67.07%)	234.74 (+66.89%)	168.85 (+65.12%)
Proposed (CMY)	50.22 (+20.52%)	55.83 (+28.20%)	210.56 (+49.07%)	215.63 (+46.77%)	102.31 (+54.90%)	217.32 (+60.78%)	211.64 (+50.46%)	151.93 (+48.57%)
Proposed (YCbCr)	61.23 (+46.94%)	62.31 (+43.08%)	234.44 (+65.98%)	242.25 (+64.89%)	118.64 (+79.62%)	226.41 (+67.50%)	229.95 (+63.48%)	167.89 (+64.18%)
Proposed (HSL)	85.43 (+105.01%)	87.99 (+102.04%)	256.71 (+81.74%)	277.38 (+88.80%)	131.46 (+99.03%)	237.94 (+76.03%)	249.89 (+77.66%)	189.54 (+85.35%)
Proposed (HSV)	64.36 (+54.45%)	65.37 (+50.10%)	237.17 (+67.91%)	241.10 (+64.10%)	120.21 (+82.00%)	224.03 (+65.74%)	232.85 (+65.54%)	169.30 (+65.56%)
Proposed (CIE XYZ)	51.12 (+22.68%)	53.45 (+22.73%)	215.11 (+52.29%)	220.92 (+50.37%)	108.71 (+64.59%)	215.65 (+59.54%)	212.06 (+50.76%)	153.86 (+50.46%)
Proposed (CIE LAB)	50.95 (+22.27%)	52.96 (+21.61%)	213.86 (+51.41%)	219.80 (+49.61%)	105.93 (+60.38%)	217.89 (+61.20%)	215.71 (+53.36%)	153.87 (+50.47%)

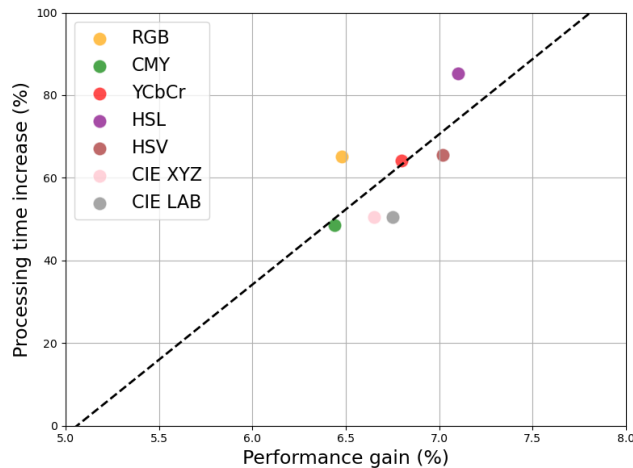


Figure 5: Relationship between average gain in performance (higher is better) and average increase in processing time (lower is better) of different color models.

methods utilized in surrogate training in SNN, both proposed method and baseline are still able to compute spike signal within linear time complexity  $\mathcal{O}(n)$  [3]. Empirical evaluation of processing speed and utilized memory could varied

across datasets, attributed to factors such as input resolution, hardware specifications, and software library versions. Also, another limitation is that, similar to recent studies [11], [28], the experiments in our study are still based on software simulations. Implementations and experiments on hardware would be definitely needed to understand the actual complexity.

As our study is the first one to investigate bit plane coding in SNNs, it can be extended in different directions. First, a more extensive theoretical analysis is necessary to model the impact of bit plane coding on the performance of SNNs for different machine learning tasks or cross ANN-SNN benchmarking [63]. Second, it is obvious that the choice of color model may depend on the task in question, such as temporal-based segmentation [64], object recognition [65] and knowledge distillation [66]. So, experiments in different application domains to understand the effects of the proposed method and color models for different tasks. Additionally for future works, the proposed method should be implemented by mapping proposed spike coding method on hardware platforms for deployment such as FPGA or Intel Loihi chip [6] and tested in practical scenarios such as low power edge devices [67].

## VII. CONCLUSION

In this paper, we have introduced a novel coding method for SNN that leverages bit planes of input image data. This approach proved to enhance the computational accuracy of SNN without increasing the model size. Through providing theoretically justified proof and extensive experimental validation, we have demonstrated the effectiveness of our coding strategy with multiple well known coding scheme across different grayscale and color datasets. This study is pioneering in the investigation of bit planes and color models within the context of SNN. We expect that the findings in this paper open new avenues for the development of more efficient and effective SNN models. In future work, we will further investigate the impacts of bit plane coding and color models in different application domains, such as medical analysis and object detection for traffic smart cameras. In addition, the proposed method will be implemented and tested on practical hardware platforms.

## ACKNOWLEDGMENTS

We are sincerely thankful for the constructive criticisms and insights of reviewers for the betterment of our research.

## DATA AVAILABILITY

Source code for our experiment is publicly available on GitHub (<https://github.com/luutn2002/bit-plane-snn>).

## References

- [1] M. A. Wani, F. A. Bhat, S. Afzal, and A. I. Khan, *Advances in deep learning*. Springer, 2020.
- [2] D.-A. Nguyen, X.-T. Tran, and F. Iacopi, “A review of algorithms and hardware implementations for spiking neural networks,” *Journal of Low Power Electronics and Applications*, vol. 11, no. 2, p. 23, 2021.
- [3] D. Auge, J. Hille, E. Mueller, and A. Knoll, “A survey of encoding techniques for signal processing in spiking neural networks,” *Neural Processing Letters*, vol. 53, no. 6, pp. 4693–4710, 2021.
- [4] P. Blouw, X. Choo, E. Hunsberger, and C. Eliasmith, “Benchmarking keyword spotting efficiency on neuromorphic hardware,” in *Proceedings of the 7th annual neuro-inspired computational elements workshop*, 2019, pp. 1–8.
- [5] B. Rajendran, A. Sebastian, M. Schmuker, N. Srinivasan, and E. Eleftheriou, “Low-power neuromorphic hardware for signal processing applications: A review of architectural and system-level design approaches,” *IEEE Signal Processing Magazine*, vol. 36, no. 6, pp. 97–110, 2019.
- [6] J. D. Nunes, M. Carvalho, D. Carneiro, and J. S. Cardoso, “Spiking neural networks: A survey,” *IEEE Access*, vol. 10, pp. 60 738–60 764, 2022.
- [7] G. Srinivasan, S. Roy, V. Raghunathan, and K. Roy, “Spike timing dependent plasticity based enhanced self-learning for efficient pattern recognition in spiking neural networks,” in *2017 International Joint Conference on Neural Networks (IJCNN)*. IEEE, 2017, pp. 1847–1854.
- [8] F. Liu, W. Zhao, Y. Chen, Z. Wang, T. Yang, and L. Jiang, “Sstdp: Supervised spike timing dependent plasticity for efficient spiking neural network training,” *Frontiers in Neuroscience*, vol. 15, p. 756876, 2021.
- [9] E. O. Neftci, H. Mostafa, and F. Zenke, “Surrogate gradient learning in spiking neural networks: Bringing the power of gradient-based optimization to spiking neural networks,” *IEEE Signal Processing Magazine*, vol. 36, no. 6, pp. 51–63, 2019.
- [10] J. K. Eshraghian, M. Ward, E. O. Neftci, X. Wang, G. Lenz, G. Dwivedi, M. Bennamoun, D. S. Jeong, and W. D. Lu, “Training spiking neural networks using lessons from deep learning,” *Proceedings of the IEEE*, 2023.
- [11] W. Fang, Z. Yu, Y. Chen, T. Huang, T. Masquelier, and Y. Tian, “Deep residual learning in spiking neural networks,” *Advances in Neural Information Processing Systems*, vol. 34, pp. 21 056–21 069, 2021.
- [12] L. Vorabbi, D. Maltoni, and S. Santi, “Input layer binarization with bit-plane encoding,” in *International Conference on Artificial Neural Networks*. Springer, 2023, pp. 395–406.
- [13] S. N. Gowda and C. Yuan, “Colornet: Investigating the importance of color spaces for image classification,” in *Computer Vision–ACCV 2018: 14th Asian Conference on Computer Vision, Perth, Australia, December 2–6, 2018, Revised Selected Papers, Part IV 14*. Springer, 2019, pp. 581–596.
- [14] J. Taipalmaa, N. Passalis, and J. Raitoharju, “Different color spaces in deep learning-based water segmentation for autonomous marine operations,” in *2020 IEEE international conference on image processing (ICIP)*. IEEE, 2020, pp. 3169–3173.
- [15] N. Luu, D. Luu, P. N. Nam, and T. C. Thang, “Improvement of spiking neural network with bit plane coding,” in *2024 IEEE 16th International Conference on Computational Intelligence and Communication Networks (CICN)*. IEEE, 2024.
- [16] H. Abelson and G. J. Sussman, *Structure and interpretation of computer programs*. The MIT Press, 1996.
- [17] D. E. Rumelhart, G. E. Hinton, and R. J. Williams, “Learning representations by back-propagating errors,” *nature*, vol. 323, no. 6088, pp. 533–536, 1986.
- [18] W. Maass, “Networks of spiking neurons: the third generation of neural network models,” *Neural networks*, vol. 10, no. 9, pp. 1659–1671, 1997.
- [19] P. A. Merolla, J. V. Arthur, R. Alvarez-Icaza, A. S. Cassidy, J. Sawada, F. Akopyan, B. L. Jackson, N. Imam, C. Guo, Y. Nakamura et al., “A million spiking-neuron integrated circuit with a scalable communication network and interface,” *Science*, vol. 345, no. 6197, pp. 668–673, 2014.
- [20] W. Gerstner and W. M. Kistler, *Spiking neuron models: Single neurons, populations, plasticity*. Cambridge university press, 2002.
- [21] C. Lee, P. Panda, G. Srinivasan, and K. Roy, “Training deep spiking convolutional neural networks with stdp-based unsupervised pre-training followed by supervised fine-tuning,” *Frontiers in neuroscience*, vol. 12, p. 435, 2018.
- [22] N. T. Luu, “Accuracy-robustness trade off via spiking neural network gradient sparsity trail,” *arXiv preprint arXiv:2509.23762*, 2025.
- [23] N. T. Luu, D. T. Luu, P. N. Nam, and T. C. Thang, “Hybrid layer-wise ann-snn with surrogate spike encoding-decoding structure,” *arXiv preprint arXiv:2509.24411*, 2025.
- [24] B. Rueckauer, I.-A. Lungu, Y. Hu, M. Pfeiffer, and S.-C. Liu, “Conversion of continuous-valued deep networks to efficient event-driven networks for image classification,” *Frontiers in neuroscience*, vol. 11, p. 682, 2017.
- [25] L. F. Abbott, “Lapicque’s introduction of the integrate-and-fire model neuron (1907),” *Brain research bulletin*, vol. 50, no. 5–6, pp. 303–304, 1999.
- [26] Y. Li, S. Deng, X. Dong, R. Gong, and S. Gu, “A free lunch from ann: Towards efficient, accurate spiking neural networks calibration,” in *International conference on machine learning*. PMLR, 2021, pp. 6316–6325.
- [27] S. Deng and S. Gu, “Optimal conversion of conventional artificial neural networks to spiking neural networks,” *arXiv preprint arXiv:2103.00476*, 2021.
- [28] Y. Hu, H. Tang, and G. Pan, “Spiking deep residual networks,” *IEEE Transactions on Neural Networks and Learning Systems*, vol. 34, no. 8, pp. 5200–5205, 2021.
- [29] P. U. Diehl, D. Neil, J. Binas, M. Cook, S.-C. Liu, and M. Pfeiffer, “Fast-classifying, high-accuracy spiking deep networks through weight and threshold balancing,” in *2015 International joint conference on neural networks (IJCNN)*. iee, 2015, pp. 1–8.
- [30] L. Zhang, S. Zhou, T. Zhi, Z. Du, and Y. Chen, “Tdsnn: From deep neural networks to deep spike neural networks with temporal-coding,” in *Proceedings of the AAAI conference on artificial intelligence*, vol. 33, no. 01, 2019, pp. 1319–1326.
- [31] M. Dampfhofer, T. Mesquida, A. Valentian, and L. Anghel, “Are snns really more energy-efficient than anns? an in-depth hardware-aware study,” *IEEE Transactions on Emerging Topics in Computational Intelligence*, vol. 7, no. 3, pp. 731–741, 2022.
- [32] K. Alex, “Learning multiple layers of features from tiny images,” <https://www.cs.toronto.edu/kriz/learning-features-2009-TR.pdf>, 2009.
- [33] K. He, X. Zhang, S. Ren, and J. Sun, “Deep residual learning for image recognition,” in *Proceedings of the IEEE conference on computer vision and pattern recognition*, 2016, pp. 770–778.
- [34] D. Huh and T. J. Sejnowski, “Gradient descent for spiking neural networks,” *Advances in neural information processing systems*, vol. 31, 2018.

[35] T. A. Ngo, T. Nguyen, and T. C. Thang, "A survey of recent advances in quantum generative adversarial networks," *Electronics*, vol. 12, no. 4, p. 856, 2023.

[36] T. Nguyen, I. Paik, Y. Watanobe, and T. C. Thang, "An evaluation of hardware-efficient quantum neural networks for image data classification," *Electronics*, vol. 11, no. 3, p. 437, 2022.

[37] T. Nguyen, I. Paik, H. Sagawa, and T. C. Thang, "Quantum machine learning with quantum image representations," in 2022 IEEE International Conference on Quantum Computing and Engineering (QCE). IEEE, 2022, pp. 851–854.

[38] Y. Liu, J. Dong, and P. Zhou, "Defending against adversarial attacks in deep learning with robust auxiliary classifiers utilizing bit-plane slicing," *ACM Journal on Emerging Technologies in Computing Systems (JETC)*, vol. 18, no. 3, pp. 1–17, 2022.

[39] G. Chen, Y. Chen, Z. Yuan, X. Lu, X. Zhu, and W. Li, "Breast cancer image classification based on cnn and bit-plane slicing," in 2019 International Conference on Medical Imaging Physics and Engineering (ICMIE). IEEE, 2019, pp. 1–4.

[40] N. A. Ibraheem, M. M. Hasan, R. Z. Khan, and P. K. Mishra, "Understanding color models: a review," *ARPN Journal of science and technology*, vol. 2, no. 3, pp. 265–275, 2012.

[41] K. N. Plataniotis, "Color image processing and applications," *Measurement Science and Technology*, vol. 12, no. 2, pp. 222–222, 2001.

[42] H.-K. Kim, J. H. Park, and H.-Y. Jung, "An efficient color space for deep-learning based traffic light recognition," *Journal of Advanced Transportation*, vol. 2018, no. 1, p. 2365414, 2018.

[43] M. Chyad, B. Zaidan, A. Zaidan, H. Pilehkoohi, R. Aalaa, S. Qahtan, H. A. Alsattar, D. Pamucar, and V. Simic, "Exploring adversarial deep learning for fusion in multi-color channel skin detection applications," *Information Fusion*, vol. 114, p. 102632, 2025.

[44] L. Deng, "The mnist database of handwritten digit images for machine learning research [best of the web]," *IEEE signal processing magazine*, vol. 29, no. 6, pp. 141–142, 2012.

[45] S. Shalev-Shwartz, O. Shamir, and S. Shammah, "Failures of gradient-based deep learning," in *International Conference on Machine Learning*. PMLR, 2017, pp. 3067–3075.

[46] S. Ghadimi and G. Lan, "Stochastic first-and zeroth-order methods for nonconvex stochastic programming," *SIAM journal on optimization*, vol. 23, no. 4, pp. 2341–2368, 2013.

[47] A. Paszke, S. Gross, F. Massa, A. Lerer, J. Bradbury, G. Chanan, T. Killeen, Z. Lin, N. Gimelshein, L. Antiga *et al.*, "Pytorch: An imperative style, high-performance deep learning library," *Advances in neural information processing systems*, vol. 32, 2019.

[48] W. Fang, Y. Chen, J. Ding, Z. Yu, T. Masquelier, D. Chen, L. Huang, H. Zhou, G. Li, and Y. Tian, "Spikingjelly: An open-source machine learning infrastructure platform for spike-based intelligence," *Science Advances*, vol. 9, no. 40, p. eadi1480, 2023. [Online]. Available: <https://www.science.org/doi/abs/10.1126/sciadv.adi1480>

[49] E. Riba, D. Mishkin, D. Ponsa, E. Rublee, and G. Bradski, "Kornia: an open source differentiable computer vision library for pytorch," in *Winter Conference on Applications of Computer Vision*, 2020. [Online]. Available: <https://arxiv.org/pdf/1910.02190.pdf>

[50] J. Kim, H. Kim, S. Huh, J. Lee, and K. Choi, "Deep neural networks with weighted spikes," *Neurocomputing*, vol. 311, pp. 373–386, 2018.

[51] D. Heeger *et al.*, "Poisson model of spike generation," *Handout*, University of Stanford, vol. 5, no. 1–13, p. 76, 2000.

[52] A. Radford, J. W. Kim, C. Hallacy, A. Ramesh, G. Goh, S. Agarwal, G. Sastry, A. Askell, P. Mishkin, J. Clark *et al.*, "Learning transferable visual models from natural language supervision," in *International conference on machine learning*. PMLR, 2021, pp. 8748–8763.

[53] N. T. Luu, C. Onuoha, and T. C. Thang, "Blind image quality assessment with multimodal prompt learning," in 2023 IEEE 15th International Conference on Computational Intelligence and Communication Networks (CICN). IEEE, 2023, pp. 614–618.

[54] D. P. Kingma and J. Ba, "Adam: A method for stochastic optimization," *arXiv preprint arXiv:1412.6980*, 2014.

[55] T. Clanuwat, M. Bober-Irizar, A. Kitamoto, A. Lamb, K. Yamamoto, and D. Ha. (2018) Deep learning for classical Japanese literature.

[56] H. Xiao, K. Rasul, and R. Vollgraf, "Fashion-mnist: a novel image dataset for benchmarking machine learning algorithms," *arXiv preprint arXiv:1708.07747*, 2017.

[57] F.-F. Li, M. Andreetto, M. Ranzato, and P. Perona, "Caltech 101," Apr 2022.

[58] G. Griffin, A. Holub, and P. Perona, "Caltech 256," Apr 2022.

[59] P. Helber, B. Bischke, A. Dengel, and D. Borth, "Eurosat: A novel dataset and deep learning benchmark for land use and land cover classification," *IEEE Journal of Selected Topics in Applied Earth Observations and Remote Sensing*, vol. 12, no. 7, pp. 2217–2226, 2019.

[60] J. Howard, "Imagenette." [Online]. Available: <https://github.com/fastai/imagenette/>

[61] L. Bossard, M. Guillaumin, and L. Van Gool, "Food-101 – mining discriminative components with random forests," in *European Conference on Computer Vision*, 2014.

[62] J. Deng, W. Dong, R. Socher, L.-J. Li, K. Li, and L. Fei-Fei, "Imagenet: A large-scale hierarchical image database," in *2009 IEEE conference on computer vision and pattern recognition*. Ieee, 2009, pp. 248–255.

[63] L. Deng, Y. Wu, X. Hu, L. Liang, Y. Ding, G. Li, G. Zhao, P. Li, and Y. Xie, "Rethinking the performance comparison between snns and anns," *Neural networks*, vol. 121, pp. 294–307, 2020.

[64] K. Patel, E. Hunsberger, S. Batir, and C. Eliasmith, "A spiking neural network for image segmentation," *arXiv preprint arXiv:2106.08921*, 2021.

[65] Q. Su, Y. Chou, Y. Hu, J. Li, S. Mei, Z. Zhang, and G. Li, "Deep directly-trained spiking neural networks for object detection," in *Proceedings of the IEEE/CVF International Conference on Computer Vision*, 2023, pp. 6555–6565.

[66] Y. Guo, W. Peng, Y. Chen, L. Zhang, X. Liu, X. Huang, and Z. Ma, "Joint a-snn: Joint training of artificial and spiking neural networks via self-distillation and weight factorization," *Pattern Recognition*, vol. 142, p. 109639, 2023.

[67] H. Zheng, Y. Guo, X. Yang, S. Xiao, and Z. Yu, "Balancing the cost and performance trade-offs in snn processors," *IEEE Transactions on Circuits and Systems II: Express Briefs*, vol. 68, no. 9, pp. 3172–3176, 2021.

[68] J. E. Littlewood and A. C. Offord, "On the number of real roots of a random algebraic equation. ii," in *Mathematical proceedings of the Cambridge philosophical society*, vol. 35, no. 2. Cambridge University Press, 1939, pp. 133–148.

[69] E. Zakon, "Mathematical analysis. volume i/zakon, elias," West Lafayette, Indiana, USA, 2004.

[70] W. G. Cochran, "The distribution of quadratic forms in a normal system, with applications to the analysis of covariance," in *Mathematical Proceedings of the Cambridge Philosophical Society*, vol. 30, no. 2. Cambridge University Press, 1934, pp. 178–191.

[71] B. Laurent and P. Massart, "Adaptive estimation of a quadratic functional by model selection," *Annals of statistics*, pp. 1302–1338, 2000.

## APPENDIX A BASIS FOR STOCHASTIC THEOREM REUSABILITY IN SNN SURROGATE TRAINING

As discussed in Section II-B, surrogate gradient methods attempt to adapt deep learning's gradient optimization techniques to SNNs, maintaining a close connection to traditional deep learning and convex optimization. Given well-established conditions and appropriate modifications, the theoretical principles from these fields can be leveraged to explain the behavior of surrogate gradient methods. To prove this viewpoint we consider a classical stochastic optimization problem associated with learning a target function  $h$  can be formulated as:

$$\min_{\mathbf{w}} F_h(\mathbf{w}) = \mathbb{E}_{\mathbf{x}} [\ell(p_{\mathbf{w}}(\mathbf{x}), h(\mathbf{x}))] \quad (13)$$

where  $\ell$  is a loss function,  $\mathbf{x}$  represents stochastic inputs (assumed to be vectors in Euclidean space), and  $p_{\mathbf{w}}$  is a differentiable predictor parameterized by  $\mathbf{w}$  (e.g., a traditional ANN of a specific architecture). It is assumed that  $\mathbb{E}_{\mathbf{x}} [\left\| \frac{\partial}{\partial \mathbf{w}} p_{\mathbf{w}} \right\|^2] \leq G(\mathbf{w})^2$  for some scalar  $G(\mathbf{w})$ , and that  $F$  is differentiable. The variance of the given cost function can be quantified as:

$$Var(\mathcal{H}, F, \mathbf{w}) = \mathbb{E}_h \|\nabla F_h(\mathbf{w}) - \mathbb{E}_{h'} \nabla F_{h'}(\mathbf{w})\|^2 \quad (14)$$

Now, we consider an example theorem along with its auxiliary lemmas derived from a theoretical analysis of a gradient-based optimization experiment [45]:

**Theorem A.1** (Shalev et al., 2017). *Let  $\mathbf{x}_1^k$  denote a  $k$ -tuple  $(\mathbf{x}_1, \dots, \mathbf{x}_k)$  of input instances, and assume that each  $\mathbf{x}_l$  is i.i.d. standard Gaussian in  $\mathbb{R}^d$ . Define*

$$h_{\mathbf{u}}(\mathbf{x}_1^k) = \prod_{l=1}^k \text{sign}(\mathbf{u}^\top \mathbf{x}_l),$$

and the objective (w.r.t. some predictor  $p_{\mathbf{w}}$  parameterized by  $\mathbf{w}$ )

$$F(\mathbf{w}) = \mathbb{E}_{\mathbf{x}_1^k} [\ell(p_{\mathbf{w}}(\mathbf{x}_1^k), h_{\mathbf{u}}(\mathbf{x}_1^k))].$$

Where the loss function  $\ell$  is either the square loss  $\ell(\hat{y}, y) = \frac{1}{2}(\hat{y} - y)^2$  or a classification loss of the form  $\ell(\hat{y}, y) = r(\hat{y} \cdot y)$  for some 1-Lipschitz function  $r$ .

Fix some  $\mathbf{w}$ , and suppose that  $p_{\mathbf{w}}(\mathbf{x})$  is differentiable w.r.t.  $\mathbf{w}$  and satisfies  $\mathbb{E}_{\mathbf{x}_1^k} [\|\frac{\partial}{\partial \mathbf{w}} p_{\mathbf{w}}(\mathbf{x}_1^k)\|^2] \leq G(\mathbf{w})^2$ . Then if  $\mathcal{H} = \{h_{\mathbf{u}} : \mathbf{u} \in \mathbb{R}^d, \|\mathbf{u}\| = 1\}$ , then

$$\text{Var}(\mathcal{H}, F, \mathbf{w}) \leq G(\mathbf{w})^2 \cdot O\left(\sqrt{\frac{k \log(d)}{d}}\right)^k.$$

**Lemma A.2** (Shalev et al., 2017). *Let  $h_1, \dots, h_n$  be real-valued functions on some Euclidean space, which belong to some weighted  $L_2$  space. Suppose that  $\|h_i\|_{L_2} = 1$  and  $\max_{i \neq j} |\langle h_i, h_j \rangle_{L_2}| \leq c$ . Then for any function  $g$  on the same domain,*

$$\frac{1}{n} \sum_{i=1}^n \langle h_i, g \rangle_{L_2}^2 \leq \|g\|_{L_2}^2 \left(\frac{1}{n} + c\right).$$

**Lemma A.3** (Shalev et al., 2017). *If  $\mathbf{w}, \mathbf{v}$  are two unit vectors in  $\mathbb{R}^d$ , and  $\mathbf{x}$  is a standard Gaussian random vector, then*

$$|\mathbb{E}_{\mathbf{x}} [\text{sign}(\mathbf{w}^\top \mathbf{x}) \text{sign}(\mathbf{v}^\top \mathbf{x})]| \leq |\langle \mathbf{w}, \mathbf{v} \rangle|$$

Theorem A.1 holds true as long as Lemma A.2 and Lemma A.3 remain valid. There are two primary approaches to generalizing this theorem for surrogate gradient methods:

- Demonstrating that as the distribution of the input  $\mathbf{x}$  have a distribution similar to a Bernoulli distribution, the lemmas remain valid, thereby ensuring the theorem holds.
- Reformulating the surrogate gradient problem as a conventional stochastic optimization problem.

We first consider the first approach. Suppose each entry  $\mathbf{x}_i$  of the vector  $\mathbf{x}$  follows a Bernoulli distribution with parameter  $p_i$ , so that the joint probability of  $\mathbf{x}$  is given by:

$$Pr(\mathbf{x}) = \prod_i p_i^{x_i} (1 - p_i)^{1 - x_i}.$$

Since the components of Lemma A.2 do not depend on the distribution of  $\mathbf{x}$ , the lemma remains unchanged. However, Lemma A.3 no longer necessarily holds, as any multiplication involving  $\mathbf{x}$  can be interpreted as a  $d$ -dimensional

Littlewood–Offord problem [68], which only admits a probabilistic upper bound rather than a deterministic one. Consequently, Lemma A.3 becomes unstable and holds only under the additional assumption that the unit vectors also follow a standard Gaussian distribution, i.e.,  $\mathbf{w}, \mathbf{v} \sim \mathcal{N}(0, 1)$ .

Under this assumption,  $w^T x$  and  $v^T x$  are jointly zero-mean Gaussian with variance 1 and covariance  $\mathbb{E}[w^T x v^T x] = w^T v$ . Thus,

$$\begin{aligned} \mathbb{E} [\text{sign}(w^T x) \text{sign}(v^T x)] &= 2 \Pr(w^T x \geq 0, v^T x \geq 0) \\ &\quad - 2 \Pr(w^T x \geq 0, v^T x \leq 0). \end{aligned} \quad (15)$$

Using the quadrant probability of bivariate normal distributions, this simplifies to:

$$\begin{aligned} &2 \left( \frac{1}{4} + \frac{\sin^{-1}(w^T v)}{2\pi} \right) - 2 \left( \frac{\cos^{-1}(w^T v)}{2\pi} \right) \\ &= \frac{2 \sin^{-1}(w^T v)}{\pi}. \end{aligned} \quad (16)$$

The absolute value of this expression is upper bounded by  $|w^T v|$ , thereby establishing the stability of Lemma A.3 as long as the condition of  $\mathbf{w}, \mathbf{v} \sim \mathcal{N}(0, 1)$  held true. However, proving each theorem along with its auxiliary lemmas under different input distributions shift would be inefficient since the theorem only hold within strictly constructed condition.

Alternatively, we can approach this by reformulating surrogate gradient method as a traditional stochastic optimization problem. In this case, our objective is defined as:

$$\begin{aligned} \min_{\mathbf{w}} F_h(\mathbf{w}) &= \mathbb{E}_{\mathbf{x}} [\ell(P_{\mathbf{w}}(\mathbf{x}), h(\mathbf{x}))], \\ P_{\mathbf{w}}(\mathbf{x}) &= \mathbb{E}_T [p_{\mathbf{w}}(e(\mathbf{x}))], \end{aligned} \quad (17)$$

where the surrogate gradient model  $P_{\mathbf{w}}(\mathbf{x})$  encodes the input  $\mathbf{x}$  into a spike signal using an encoding function  $e(\mathbf{x})$  and computes the expected output signal across the time dimension  $T$  to generate the final stochastic prediction. Using this reformulation, we ensure that as long as the encoding function  $e(\mathbf{x})$  is differentiable, all conventional deep learning theorems remain applicable to the surrogate gradient model. If  $e(\mathbf{x})$  is not differentiable, the theorem holds only if its components and auxiliary lemmas do not require gradient computation with respect to  $\mathbf{x}$ . In similar manner with Equation 10, gradient of coding function  $\frac{\partial e(\mathbf{x})}{\partial \mathbf{x}}$  is not required and Equation 10 can be apply to surrogate SNN model as is.

## APPENDIX B PROOF FOR SNR INEQUALITY

Firstly, we will provide some background knowledge to assist our mathematical derivation of Equation 11. Given a SNN model that employ hard-reset IF neurons with backpropagate through time (BPTT) [10], [11], [22], [23], [48], optimization

scheme is defined as:

$$\begin{aligned} u_i^{(l)}(t) &= (1 - s_i^{(l-1)}(t-1)) u_i^{(l)}(t-1) \\ &\quad + W^{(l)} s^{(l-1)}(t) + b_i^{(l)}, \\ s_i^{(l)}(t) &= \Theta \left( u_i^{(l)}(t), V_{th} \right) \\ \Theta(x, V_{th}) &= \begin{cases} 1 & \text{if } x - V_{th} \geq 0 \\ 0 & \text{otherwise} \end{cases} \\ \frac{\partial \mathcal{L}}{\partial W^{(l)}} &= \sum_{t=1}^T \frac{\partial \mathcal{L}}{\partial s^{(l)}(t)} \cdot \frac{\partial s^{(l)}(t)}{\partial u^{(l)}(t)} \cdot \frac{\partial u^{(l)}(t)}{\partial W^{(l)}} \end{aligned} \quad (18)$$

where:

- $u_i^{(l)}(t)$  is the membrane potential of neuron  $i$  in layer  $l$  at time  $t \in T$ ,
- $s_i^{(l)}(t)$  is the spike output of neuron  $i$ , similarly with prior layer signal  $s_i^{(l-1)}(t)$ ,
- $V_{th}$  is the threshold voltage,
- synaptic weight  $W^{(l)}$  and bias  $b_i^{(l)}$ ,
- $\Theta$  is the Heaviside function,
- loss function  $\mathcal{L}$  and its gradient with respect to weight  $\frac{\partial \mathcal{L}}{\partial W^{(l)}}$ .

As noted from Appendix A, SNR expression denoted in Equation 10 [45] is adaptable to surrogate SNN model by substitute results from Equation 18 as:

$$\begin{aligned} SNR(\delta(\mathbf{x})) &= \frac{\|\mathbb{E}_{\mathbf{x}}[\delta(\mathbf{x})]\|_2^2}{\mathbb{E}_{\mathbf{x}}\|\delta(\mathbf{x}) - \mathbb{E}_{\mathbf{x}}[\delta(\mathbf{x})]\|_2^2}, \\ \delta(\mathbf{x}) &= h(\mathbf{x}) \cdot g_{\mathbf{w}}^T(\mathbf{x}) \\ &= h(\mathbf{x}) \cdot \sum_{t=1}^T \frac{\partial s^{(l)}(t)}{\partial u^{(l)}(t)} \cdot \frac{\partial u^{(l)}(t)}{\partial W^{(l)}} \end{aligned} \quad (19)$$

where  $g_{\mathbf{w}}(\mathbf{x}) = \frac{\partial}{\partial \mathbf{w}} p_{\mathbf{w}}(\mathbf{x})$  is the Jacobian of model  $p_{\mathbf{w}}(\mathbf{x})$  with respect to model weight  $\mathbf{w}$ . Under the case of signal concatenation with bit plane coding of length  $N_{bit}$ , we would have  $\delta^{bit}(\mathbf{x})$ :

$$\begin{aligned} \delta^{bit}(\mathbf{x}) &= h(\mathbf{x}) \cdot \left( \sum_{t=1}^T \frac{\partial s^{(l)}(t)}{\partial u^{(l)}(t)} \cdot \frac{\partial u^{(l)}(t)}{\partial W^{(l)}} \right. \\ &\quad \left. + \sum_{t=1}^{N_{bit}} \frac{\partial s^{(l)}(t)}{\partial u^{(l)}(t)} \cdot \frac{\partial u^{(l)}(t)}{\partial W^{(l)}} \right) \\ &= h(\mathbf{x}) \cdot g_{\mathbf{w}}^T(\mathbf{x}) + h(\mathbf{x}) \cdot g_{\mathbf{w}}^{bit}(\mathbf{x}) \\ &= h(\mathbf{x}) \cdot g_{\mathbf{w}}^{T+bit}(\mathbf{x}) \end{aligned} \quad (20)$$

Equation 11 hold true if the following theorem is true:

**Theorem B.1.** Assume that bit channels concatenated gradient  $g_{\mathbf{w}}^{bit}(\mathbf{x})$  does not explode nor vanish, bounded as:

$$G(\mathbf{w})^2 > \|\mathbb{E}_{\mathbf{x}}[g_{\mathbf{w}}^{bit}(\mathbf{x})]\|_{\infty} > 0$$

for some scalar  $G(\mathbf{w})$ , where both gradient of baseline SNN  $g_{\mathbf{w}}^T(\mathbf{x})$  and bit plane code concatenated SNN  $g_{\mathbf{w}}^{bit}(\mathbf{x})$

converge toward a reasonable approximation of  $h(\mathbf{x})$  and have similar distribution that satisfy:

$$\begin{aligned} \text{Cov}(h(\mathbf{x}), g_{\mathbf{w}}^{bit}(\mathbf{x})) &= 0, \quad \text{sign}(\mathbb{E}_{\mathbf{x}}[h(\mathbf{x})]) > 0, \\ h(\mathbf{x}) \cdot g_{\mathbf{w}}^{T+bit}(\mathbf{x}) &\sim h(\mathbf{x}) \cdot g_{\mathbf{w}}(\mathbf{x}), \end{aligned}$$

there exist:

$$\sup(SNR(\delta^{bit}(\mathbf{x}))) \geq \sup(SNR(\delta(\mathbf{x}))).$$

where:

$$\sup(SNR(\delta^{bit}(\mathbf{x}))) = \frac{\|\mathbb{E}_{\mathbf{x}}[\delta^{bit}(\mathbf{x})]\|_{\infty}^2}{\mathbb{E}_{\mathbf{x}}\|\delta^{bit}(\mathbf{x}) - \mathbb{E}_{\mathbf{x}}[\delta^{bit}(\mathbf{x})]\|_{\infty}^2},$$

$$\sup(SNR(\delta(\mathbf{x}))) = \frac{\|\mathbb{E}_{\mathbf{x}}[\delta(\mathbf{x})]\|_{\infty}^2}{\mathbb{E}_{\mathbf{x}}\|\delta(\mathbf{x}) - \mathbb{E}_{\mathbf{x}}[\delta(\mathbf{x})]\|_{\infty}^2}$$

*Proof.* In order to prove Theorem B.1, we first need some auxiliary lemmas to be proven.

**Lemma B.2.** Assuming bit plane concatenated SNN model  $p_{\mathbf{w}}^{bit}(\mathbf{x})$  reasonably approximate  $h(\mathbf{x})$  such that bit-plane Jacobian  $g_{\mathbf{w}}^{bit}(\mathbf{x})$  satisfy:

$$\text{Cov}(h(\mathbf{x}), g_{\mathbf{w}}^{bit}(\mathbf{x})) = 0, \quad \text{sign}(\mathbb{E}_{\mathbf{x}}[h(\mathbf{x})]) > 0,$$

while bit plane gradient does not explode nor vanish over stochastic estimation, bounded as:

$$G(\mathbf{w})^2 > \|\mathbb{E}_{\mathbf{x}}[g_{\mathbf{w}}^{bit}(\mathbf{x})]\|_{\infty} > 0 \quad (21)$$

for some scalar  $G(\mathbf{w})$ , there exist:

$$\|\mathbb{E}_{\mathbf{x}}[\delta^{bit}(\mathbf{x})]\|_{\infty}^2 \geq \|\mathbb{E}_{\mathbf{x}}[\delta(\mathbf{x})]\|_{\infty}^2.$$

*Proof.* In order for the resulted inequality in our lemma exist, we need to prove that under given condition, there exist:

$$\begin{cases} \sup(\mathbb{E}_{\mathbf{x}}[\delta^{bit}(\mathbf{x})]) \geq \sup(\mathbb{E}_{\mathbf{x}}[\delta(\mathbf{x})]), \\ \inf(\mathbb{E}_{\mathbf{x}}[\delta^{bit}(\mathbf{x})]) \leq \inf(\mathbb{E}_{\mathbf{x}}[\delta(\mathbf{x})]). \end{cases}$$

As noted from initial condition in Equation 21, we have:

$$\begin{aligned} G(\mathbf{w})^2 &> \|\mathbb{E}_{\mathbf{x}}[g_{\mathbf{w}}^{bit}(\mathbf{x})]\|_{\infty} > 0 \\ \Leftrightarrow \sup(\mathbb{E}_{\mathbf{x}}[g_{\mathbf{w}}^{bit}(\mathbf{x})]) &\geq 0 \\ \Leftrightarrow \sup(\mathbb{E}_{\mathbf{x}}[h(\mathbf{x})]) \cdot \sup(\mathbb{E}_{\mathbf{x}}[g_{\mathbf{w}}^{bit}(\mathbf{x})]) &\geq 0 \\ \Leftrightarrow \sup(\mathbb{E}_{\mathbf{x}}[h(\mathbf{x})] \cdot \mathbb{E}_{\mathbf{x}}[g_{\mathbf{w}}^{bit}(\mathbf{x})] + \text{Cov}(h(\mathbf{x}), g_{\mathbf{w}}^{bit}(\mathbf{x}))) &\geq 0 \\ \Leftrightarrow \sup(\mathbb{E}_{\mathbf{x}}[h(\mathbf{x}) \cdot g_{\mathbf{w}}^{bit}(\mathbf{x})]) &\geq 0 \\ \Leftrightarrow \sup(\mathbb{E}_{\mathbf{x}}[h(\mathbf{x}) \cdot g_{\mathbf{w}}^T(\mathbf{x})]) + \sup(\mathbb{E}_{\mathbf{x}}[h(\mathbf{x}) \cdot g_{\mathbf{w}}^{bit}(\mathbf{x})]) & \\ &\geq \sup(\mathbb{E}_{\mathbf{x}}[h(\mathbf{x}) \cdot g_{\mathbf{w}}^T(\mathbf{x})]) \end{aligned}$$

Under the property of expectation's sum and Minkowski's sum [69]:

$$\begin{aligned} \Leftrightarrow \sup(\mathbb{E}_{\mathbf{x}}[h(\mathbf{x}) \cdot g_{\mathbf{w}}^{T+bit}(\mathbf{x})]) &\geq \sup(\mathbb{E}_{\mathbf{x}}[h(\mathbf{x}) \cdot g_{\mathbf{w}}^T(\mathbf{x})]) \\ \Leftrightarrow \sup(\mathbb{E}_{\mathbf{x}}[\delta^{bit}(\mathbf{x})]) &\geq \sup(\mathbb{E}_{\mathbf{x}}[\delta(\mathbf{x})]). \end{aligned}$$

We can then use a similar process with infimum inequality of initial condition:

$$\begin{aligned}
 G(\mathbf{w})^2 &> \|\mathbb{E}_{\mathbf{x}}[g_{\mathbf{w}}^{bit}(\mathbf{x})]\|_{\infty}^2 > 0 \\
 \Leftrightarrow \inf(\mathbb{E}_{\mathbf{x}}[g_{\mathbf{w}}^{bit}(\mathbf{x})]) &\leq 0 \\
 \Leftrightarrow \inf(\mathbb{E}_{\mathbf{x}}[h(\mathbf{x})]) \cdot \inf(\mathbb{E}_{\mathbf{x}}[g_{\mathbf{w}}^{bit}(\mathbf{x})]) &\leq 0 \\
 \Leftrightarrow \inf(\mathbb{E}_{\mathbf{x}}[h(\mathbf{x})] \cdot \mathbb{E}_{\mathbf{x}}[g_{\mathbf{w}}^{bit}(\mathbf{x})] + Cov(h(\mathbf{x}), g_{\mathbf{w}}^{bit}(\mathbf{x}))) &\leq 0 \\
 \Leftrightarrow \inf(\mathbb{E}_{\mathbf{x}}[h(\mathbf{x}) \cdot g_{\mathbf{w}}^{bit}(\mathbf{x})]) &\leq 0 \\
 \Leftrightarrow \inf(\mathbb{E}_{\mathbf{x}}[h(\mathbf{x}) \cdot g_{\mathbf{w}}^T(\mathbf{x})]) + \inf(\mathbb{E}_{\mathbf{x}}[h(\mathbf{x}) \cdot g_{\mathbf{w}}^{bit}(\mathbf{x})]) &\leq \inf(\mathbb{E}_{\mathbf{x}}[h(\mathbf{x}) \cdot g_{\mathbf{w}}^T(\mathbf{x})]) \\
 \Leftrightarrow \inf(\mathbb{E}_{\mathbf{x}}[h(\mathbf{x}) \cdot g_{\mathbf{w}}^{T+bit}(\mathbf{x})]) &\leq \inf(\mathbb{E}_{\mathbf{x}}[h(\mathbf{x}) \cdot g_{\mathbf{w}}^T(\mathbf{x})]) \\
 \Leftrightarrow \inf(\mathbb{E}_{\mathbf{x}}[\delta^{bit}(\mathbf{x})]) &\leq \inf(\mathbb{E}_{\mathbf{x}}[\delta(\mathbf{x})])
 \end{aligned}$$

From here we can conclude that there exist:

$$\|\mathbb{E}_{\mathbf{x}}[\delta^{bit}(\mathbf{x})]\|_{\infty}^2 \geq \|\mathbb{E}_{\mathbf{x}}[\delta(\mathbf{x})]\|_{\infty}^2$$

under given condition.  $\square$

**Lemma B.3.** Assuming both gradient of baseline SNN  $g_{\mathbf{w}}(\mathbf{x})$  and bit plane code concatenated SNN  $g_{\mathbf{w}}^{bit}(\mathbf{x})$  converge toward a reasonable approximation of  $h(\mathbf{x})$  and have similar distribution that satisfy:

$$h(\mathbf{x}) \cdot g_{\mathbf{w}}^{T+bit}(\mathbf{x}) \sim h(\mathbf{x}) \cdot g_{\mathbf{w}}(\mathbf{x}),$$

there exist:

$$\mathbb{E}_{\mathbf{x}}\|\delta^{bit}(\mathbf{x}) - \mathbb{E}_{\mathbf{x}}[\delta^{bit}(\mathbf{x})]\|_{\infty}^2 = \mathbb{E}_{\mathbf{x}}\|\delta(\mathbf{x}) - \mathbb{E}_{\mathbf{x}}[\delta(\mathbf{x})]\|_{\infty}^2.$$

*Proof.* Since we have the initial condition that:

$$h(\mathbf{x}) \cdot g_{\mathbf{w}}^{T+bit}(\mathbf{x}) \sim h(\mathbf{x}) \cdot g_{\mathbf{w}}(\mathbf{x}),$$

then:

$$\begin{aligned}
 g_{\mathbf{w}}^{T+bit}(\mathbf{x}) &\sim g_{\mathbf{w}}(\mathbf{x}) \\
 \Leftrightarrow \text{Var}(\delta^{bit}(\mathbf{x})) &= \text{Var}(\delta(\mathbf{x})) \\
 \Leftrightarrow \|\delta^{bit}(\mathbf{x}) - \mathbb{E}_{\mathbf{x}}[\delta^{bit}(\mathbf{x})]\|_{\infty}^2 &= \|\delta(\mathbf{x}) - \mathbb{E}_{\mathbf{x}}[\delta(\mathbf{x})]\|_{\infty}^2 \\
 \Leftrightarrow \mathbb{E}_{\mathbf{x}}\|\delta^{bit}(\mathbf{x}) - \mathbb{E}_{\mathbf{x}}[\delta^{bit}(\mathbf{x})]\|_{\infty}^2 &= \mathbb{E}_{\mathbf{x}}\|\delta(\mathbf{x}) - \mathbb{E}_{\mathbf{x}}[\delta(\mathbf{x})]\|_{\infty}^2. \tag{22}
 \end{aligned}$$

$\square$

From results of Lemma B.2 and B.3, we can conclude that there exist:

$$\begin{aligned}
 \frac{\|\mathbb{E}_{\mathbf{x}}[\delta^{bit}(\mathbf{x})]\|_{\infty}^2}{\mathbb{E}_{\mathbf{x}}\|\delta^{bit}(\mathbf{x}) - \mathbb{E}_{\mathbf{x}}[\delta^{bit}(\mathbf{x})]\|_{\infty}^2} &\geq \frac{\|\mathbb{E}_{\mathbf{x}}[\delta(\mathbf{x})]\|_{\infty}^2}{\mathbb{E}_{\mathbf{x}}\|\delta(\mathbf{x}) - \mathbb{E}_{\mathbf{x}}[\delta(\mathbf{x})]\|_{\infty}^2} \\
 \Leftrightarrow \sup(SNR(\delta^{bit}(\mathbf{x}))) &\geq \sup(SNR(\delta(\mathbf{x}))). \tag{23}
 \end{aligned}$$

$\square$

On the other hand, there are special situation where the  $L_2$  norm  $\|\delta(\mathbf{x})\|_2$  directly scale with model Jacobian  $g_{\mathbf{w}}(\mathbf{x})$  dimensions. If target function  $h(\mathbf{x})$  is zero mean normally distributed  $\mathcal{N}(0, \sigma_h^2)$ ,  $g_{\mathbf{w}}(\mathbf{x})$  have sufficiently small variance and does not saturate,  $\delta(\mathbf{x})$  would follow a zero mean normal

distribution (denoted  $\mathcal{N}(0, \sigma_{\delta}^2)$ ) and its norm can be directly decomposed to:

$$\|\delta(\mathbf{x})\|_2 = \sqrt{\sum_{i=1}^{n_1^{\delta}} \sum_{j=1}^{n_2^{\delta}} \delta_{ij}^2}.$$

where each squared entry  $\delta_{ij}^2$  would follow a chi-squared distribution with 1 degree of freedom with  $\delta_{ij}^2 \sim \sigma_{\delta}^2 \chi^2(1)$ , the sum of all squared entries follows a chi-squared distribution with  $n_1^{\delta} n_2^{\delta}$  degrees of freedom (by Cochran's theorem [70]):

$$\sum_{i=1}^{n_1^{\delta}} \sum_{j=1}^{n_2^{\delta}} \delta_{ij}^2 \sim \sigma_{\delta}^2 \chi^2(n_1^{\delta} n_2^{\delta}).$$

From the expectation property of the chi-squared distribution where  $\chi^2(n_1^{\delta} n_2^{\delta}) \sim \text{Gamma}(\alpha = nk/2, \theta = 2/n)$  of  $n$  samples with  $k$  degrees of freedom, we have:

$$E[\sigma_{\delta}^2 \chi^2(n_1^{\delta} n_2^{\delta})] = \sigma_{\delta}^2 n_1^{\delta} n_2^{\delta}.$$

Taking the square root gives:

$$\|\delta(\mathbf{x})\|_2 \approx |\sigma_{\delta}| \sqrt{n_1^{\delta} n_2^{\delta}}.$$

Thus,  $\|\delta(\mathbf{x})\|_2$  grows asymptotically as  $O(|\sigma_{\delta}| \sqrt{n_1^{\delta} n_2^{\delta}})$ . We can also quantify the probability for lower bound and upper bound of  $\|\delta(\mathbf{x})\|$  using the consequences of the standard Laurent-Massart bounds [71]:

$$\begin{aligned}
 k &= n_1^{\delta} n_2^{\delta} \\
 A := \|\delta(\mathbf{x})\|_2 &\in [\sigma_{\delta}^2 k - 2\sigma_{\delta}^2 k^{\frac{1}{2+\alpha}}, \\
 &\quad \sigma_{\delta}^2 k + 2\sigma_{\delta}^2 k^{\frac{1}{2+\alpha}} + 2\sigma_{\delta}^2 k^{\alpha}] \\
 Pr(A) &\geq 1 - e^{-k^{\alpha}} \quad (\forall \alpha \in \mathbb{R})
 \end{aligned} \tag{23}$$

It is clear that as  $k$  increase, lower bound, upper bound of  $\|\delta(\mathbf{x})\|_2$  and probability of  $\|\delta(\mathbf{x})\|_2$  is within the established range also increase.

...